



PERGAMON

International Journal of Heat and Mass Transfer 42 (1999) 4117–4130

International Journal of  
**HEAT and MASS  
TRANSFER**

www.elsevier.com/locate/ijhmt

# Direct simulation of natural convection cooling in a vertical circular cylinder

Wenxian Lin\*, S.W. Armfield

*Department of Mechanical and Mechatronic Engineering, The University of Sydney, Sydney, NSW 2006, Australia*

Received 12 August 1998; received in revised form 15 February 1999

## Abstract

The transient processes of cooling-down and stratifying an initially homogeneous fluid by natural convection in a vertical circular cylinder have been investigated numerically. The transient flow patterns are identified by the visualization of the transient evolving processes in the cylinder. The results show that vigorous flow activities concentrate mainly in the vertical thermal boundary layer along the sidewall and in the horizontal region which is the lower part of the domain where the cold intrusion flow is embedded. The transient flow patterns at the unsteady and quasi-steady stages are analysed, including the activities of the travelling waves in the vertical thermal boundary layer along the sidewall and the cold intrusions in the horizontal region. A scaling analysis is used to characterize the development of the vertical thermal boundary layer on the sidewall and the stratification in the cylinder. It is found that the numerical solutions agree very well with the scaling results. © 1999 Elsevier Science Ltd. All rights reserved.

## 1. Introduction

Natural convection driven by buoyancy arising from an imposed horizontal density gradient is widely encountered in nature and in engineering situations, such as horizontal transport in water bodies, stratification processes in thermosyphon systems, crystal growth procedures, etc. In many of these and other applications, the buoyancy is unsteady, and the response of the system to changing conditions, especially to suddenly changing boundary conditions, is of fundamental interest.

The most studied form of this problem is the case of a rectangular cavity with differentially heated sidewalls. Batchelor [1] first addressed the steady-state version of

this problem. Since then, extensive experimental, numerical and analytical studies have been conducted on the topic. Much of this work is summarized in the reviews by Catton [2] and Ostrach [3]. In spite of frequent occurrences of the unsteady case, however, the imposition of unsteady boundary conditions was evidently not considered in any detail until Patterson and Imberger [4] discussed the case of instantaneous heating and cooling of the opposing sidewalls in a rectangular cavity. In that work, they investigated the transient features that occur when the temperatures at the opposing two vertical sidewalls are impulsively heated and cooled by an equal amount, and based on the relative values of  $Ra$  and various combinations of  $Pr$  and  $A$ , they devised a classification of the development of the flow through several transient flow regimes to one of three steady-state types of flow. This flow model has since occupied the center stage of research into understanding natural convection in cavities and numerous investigations subsequently focused on

\* Corresponding author. Tel.: +61-2-9351-2591; fax: +61-2-9351-7060.

E-mail address: lin@orr.mech.eng.usyd.edu.au (W. Lin)

**Nomenclature**

$A$	aspect ratio, $H/R$
$C_d, C_s$	constants of proportionality
$C_t$	
$g$	acceleration due to gravity
$H$	height of cylinder
$n$	last time step number
$p$	pressure
$Pr$	Prandtl number, $\nu/\kappa$
$Q$	heat flux through thermal boundary layer
$R$	radius of cylinder
$Ra$	Rayleigh number, $g\beta H^3 \Delta T / \nu \kappa$
$t$	time
$T$	temperature
$u$	velocity in $r$ direction
$v$	velocity in $z$ direction
$U$	characteristic velocity, $\kappa Ra^{1/2} / H$
$r$	radial coordinate
$z$	vertical coordinate

*Greek symbols*

$\beta$	coefficient of thermal expansion
$\delta_T$	thickness of vertical thermal boundary layer
$\kappa$	thermal conductivity
$\nu$	kinematic viscosity
$\rho$	density
$\Delta t$	time step
$\Delta T$	$T_a - T_w$

*Superscript*

*	dimensional quantity
---	----------------------

*Subscripts*

a	value at ambient
w	value at sidewall
z	value at filling height

diverse aspects of the model. Nicolette and Yang [5] made a numerical and experimental investigation into two-dimensional transient natural convection of single-phase fluids inside a completely filled square enclosed with one vertical wall cooled and the other three walls insulated. Schladow et al. [6] conducted a series of two- and three-dimensional numerical simulations of transient flow in a side-heated cavity and their simulations generally agree with the results of the scaling arguments of Patterson and Imberger [4]. The numerical study by Hyun [7] on the effect of  $Pr$  on heatup of a stratified fluid in an enclosure revealed that the evolution of the flow and temperature fields are influenced by  $Pr$ . Patterson and Armfield [8] conducted detailed experimental and numerical investigations into the presence of travelling wave instabilities on the vertical-wall boundary layers and horizontal intrusions, the existence of a rapid flow divergence in the region of the outflow of the intrusions, and the presence of cavity-scale oscillations caused by the interaction of the intrusion with the opposing vertical boundary layer. Furthermore, Armfield et al. [9–12] made further in-depth studies on the wave and stability properties of the boundary layers in the cavities. The studies on unsteady natural convection in an enclosure until 1994 are well-documented in the review by Hyun [13]. Recently, Xin and Le Quéré [14] investigated numerically chaotic natural convection in a differentially heated air-filled cavity with adiabatic horizontal walls and Brooker et al. [15] conducted a non-parallel linear stability analysis of the vertical boundary layer in a differentially heated cavity.

The studies of the transient unsteady process of cooling down and stratifying a homogeneous fluid by natural convection in a vertical circular cylinder are rare. Otis and Roessler [16] conducted an experimental investigation into the development of stratification of gas in a cylindrical enclosure and provided experimental support for the existence of internal waves and revealed several time constants that characterize the process. Sakurai and Matsuda [17] conducted a theoretical investigation into the transient process in an already stratified fluid and their analysis clearly revealed the core of the intricate physics involved in the transient adjustment process of a stratified fluid system in response to changes in thermal boundary conditions in a vertical circular cylinder. This analysis was further modified and extended by Jischke and Doty [18]. Numerical investigation on this topic was addressed by Hyun et al. [19–21] who obtained finite-difference numerical solutions of the complete time-dependent, Navier–Stokes equations describing the transient process of the Sakurai and Matsuda model. All these studies have focused on the situations in which, at the initial state, the fluid is already stratified. However, the transient evolving process from the initial state of non-stratification, e.g., a homogeneous fluid, to a finally stratified state possesses some characteristically different features and this transient process is of interest from the standpoint of both basic fluid dynamics and practical applications, as the production of a stratified fluid system of any strength is usually initialized using a homogeneous fluid. On this topic, only the experimental study mentioned above [16] and

numerical studies by Hyun [22] and by Kwak et al. [23] are found. In [22], the flow and temperature structures of the heat-up process of an initially homogeneous fluid in a cylinder with a linearly-heated sidewall were elucidated using a finite-difference model. In [23], a numerical study was conducted to investigate the transient natural convective cool-down process of a fluid in a cylindrical container, with emphasis on the flow patterns when the maximum density temperature is experienced. In that work the developing flow was considered to take place in four phases, and it was shown that the total development time for each phase could be scaled against  $Ra$  and  $A$  using the relations first suggested in Patterson and Imberger [4]. Rayleigh numbers in the range  $1 \times 10^5$ – $1 \times 10^7$  were considered. In [23] the Rayleigh number is based on the radius, the maximum equivalent Rayleigh number based on height, as it is defined here, was  $1 \times 10^7$  for  $A = 1$  domain, and  $1 \times 10^8$  for  $A = 10$  domains.

In this work, the transient processes of cooling-down and stratifying an initially homogeneous fluid in a vertical circular cylinder have been investigated numerically. Flows with Rayleigh numbers up to  $6 \times 10^9$  are calculated, considerably extending the range considered by previous studies. The higher Rayleigh number flow is shown to have the same general behaviour as that observed in lower Rayleigh number studies, however, with considerably more intrusion activity. A physical scaling analysis is used to obtain relations describing the rate of development of the transient flow, again extending previous work where only the development time for each phase was considered. The scaling results are shown to agree well with the numerical simulations.

## 2. Numerical method

### 2.1. Governing equations

Under consideration is the natural convection flow in a vertical circular cylinder with a height of  $H$  and a radius of  $R$ . The top and bottom walls of the cylinder are thermally insulated. Initially the fluid in the cylinder is at rest and isothermal ( $T = T_a$ ) and at  $t = 0$  the sidewall is cooled impulsively to  $T = T_w (T_w < T_a)$ , and this temperature is maintained thereafter. Due to the symmetry, the flow in the cylinder is axisymmetric and two dimensional and the computational domain sketched in Fig. 1 is appropriate. The governing equations are the 2-D Navier–Stokes equations and the temperature equation, with the Boussinesq assumption allowing the incompressible form to be used. The equations are written in conservative, non-dimensional form in cylindrical coordinates as follows:

$$\frac{1}{r} \frac{\partial(ru)}{\partial r} + \frac{\partial v}{\partial z} = 0, \tag{1}$$

$$\frac{\partial u}{\partial t} + \frac{1}{r} \frac{\partial(ruu)}{\partial r} + \frac{\partial(vu)}{\partial z} = -\frac{\partial p}{\partial r} + \frac{Pr}{Ra^{1/2}} \times \left\{ \frac{\partial}{\partial r} \left[ \frac{1}{r} \frac{\partial(ru)}{\partial r} \right] + \frac{\partial^2 u}{\partial z^2} \right\}, \tag{2}$$

$$\frac{\partial v}{\partial t} + \frac{1}{r} \frac{\partial(ruv)}{\partial r} + \frac{\partial(vv)}{\partial z} = -\frac{\partial p}{\partial z} + \frac{Pr}{Ra^{1/2}} \times \left[ \frac{1}{r} \frac{\partial}{\partial r} \left( r \frac{\partial v}{\partial r} \right) + \frac{\partial^2 v}{\partial z^2} \right] + PrT, \tag{3}$$

$$\frac{\partial T}{\partial t} + \frac{1}{r} \frac{\partial(ruT)}{\partial r} + \frac{\partial(vT)}{\partial z} = \frac{1}{Ra^{1/2}} \times \left[ \frac{1}{r} \frac{\partial}{\partial r} \left( r \frac{\partial T}{\partial r} \right) + \frac{\partial^2 T}{\partial z^2} \right]. \tag{4}$$

In these equations, velocity is non-dimensionalized by  $U$ , time by  $H/U$ , length by  $H$ , pressure by  $\rho U^2$ , and  $(T - T_a)$  by  $\Delta T$  ( $\Delta T = T_a - T_w$ ). According to the scaling of Patterson and Imberger [4],  $U$  may be defined using the length scale of the thermal boundary layer, that is  $U = \kappa Ra^{1/2} / H$ .

The associated initial and boundary conditions are

$$u = v = 0, \quad T = 0 \quad \text{at all } r, z \quad \text{and } t < 0, \tag{5}$$

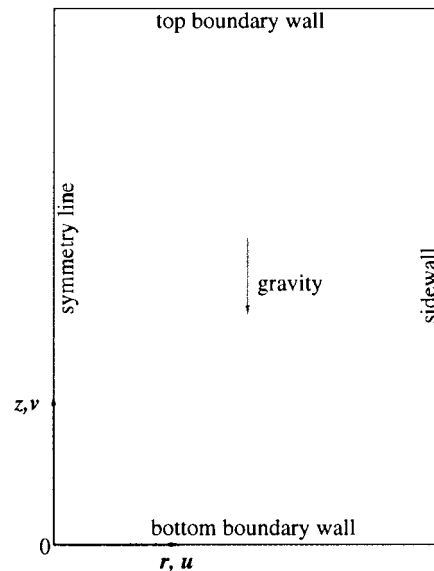


Fig. 1. Computational domain and coordinate system.

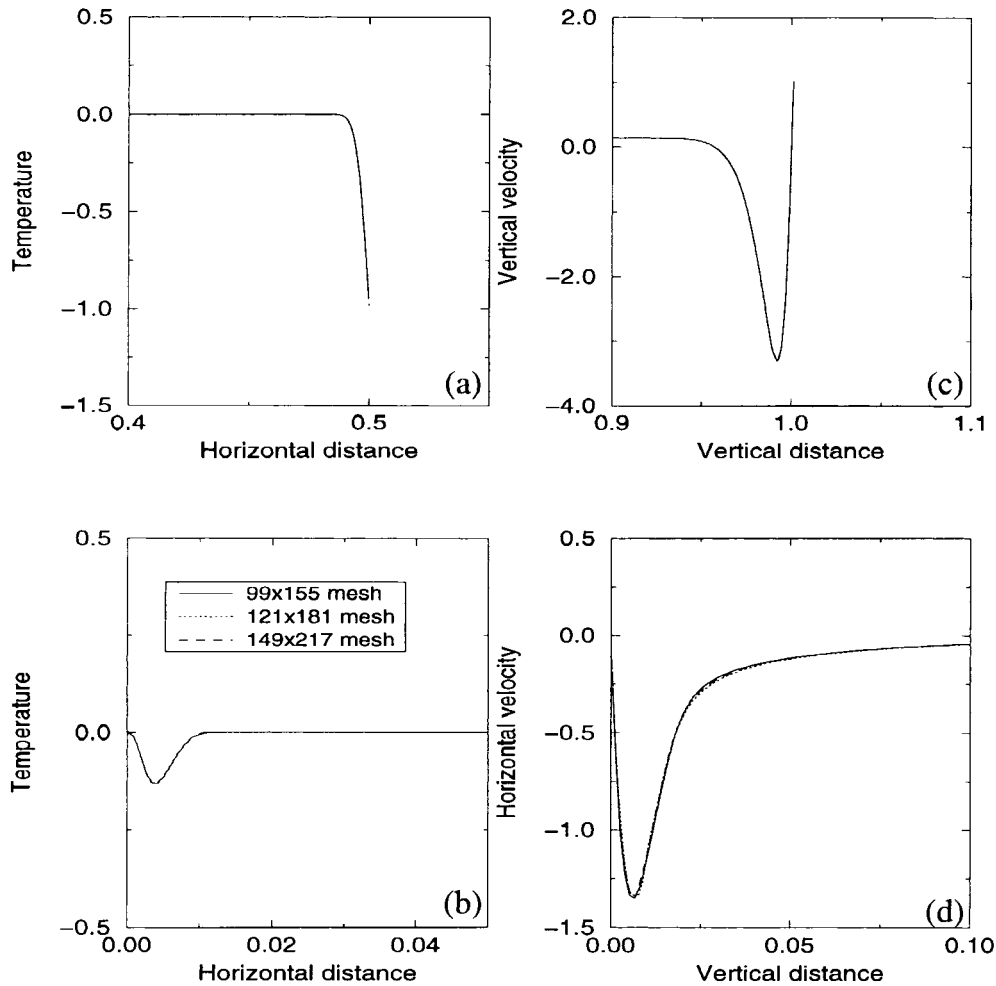


Fig. 2. Comparison of the results from the  $99 \times 155$  basic mesh,  $121 \times 181$  mesh and  $149 \times 217$  mesh for the horizontal profiles of (a) temperature and (b) vertical velocity at mid-depth  $z = 0.25$ , and  $t = 0.875$  and for the vertical profiles of (c) temperature and (d) horizontal velocity across the cold intrusion, at the location  $r = 0.4585$ , and  $t = 0.875$ .

$$u = v = 0, \quad \frac{\partial T}{\partial z} = 0 \quad \text{on } z = 0, 1, \quad (6)$$

$$u = 0, \quad \frac{\partial v}{\partial r} = \frac{\partial T}{\partial r} = 0 \quad \text{on } r = 0, \quad (7)$$

$$u = v = 0, \quad T = -1 \quad \text{on } r = 1/A \quad \text{for } t \geq 0. \quad (8)$$

## 2.2. Discretization

Because of the large variation in length scales it is necessary to use a mesh that concentrates points in the boundary layer and is relatively coarse in the interior. The meshes are constructed using a stretched grid. The basic mesh uses  $99 \times 155$  grid points (here  $A = 2$ ), which are distributed symmetrically with respect to the

domain half-width and half-height. The nearest grid-point is located 0.002 of the domain width from the wall or the symmetry line. Subsequently, the mesh expands at a rate of 7.6% up to  $r = 0.05$ , just beyond the edge of the boundary layer. After that, the mesh size expansion rate decreases until it reaches zero, resulting in a constant coarse mesh in the interior of the domain.

The equations are discretized on a non-staggered mesh in which all variables are stored at the same grid locations. The method of obtaining the pressure and satisfying continuity is similar to the SIMPLE schemes used with the conventional staggered mesh [24] but with regularizing terms included in the Poisson equation for pressure to ensure the discrete scheme is strongly elliptic. Comparisons between staggered and non-staggered solutions indicate both schemes have an

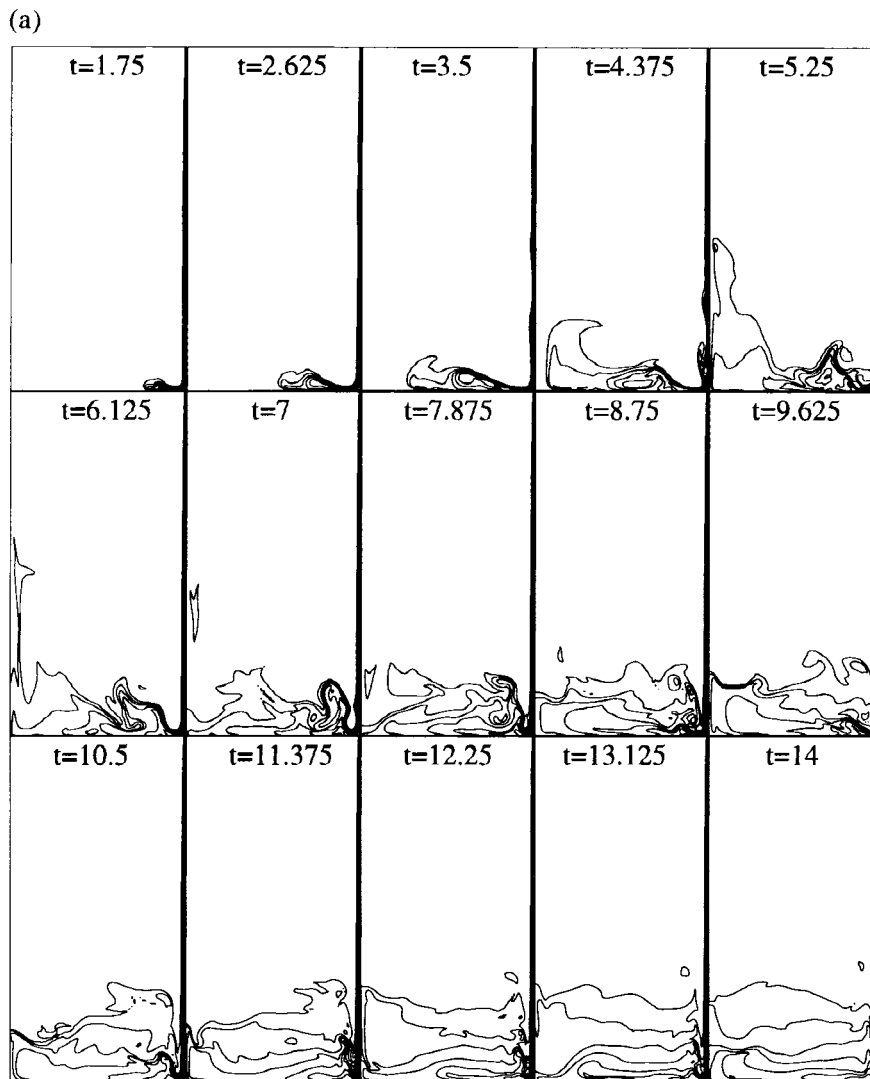


Fig. 3. (a) Time evolution of the contours of transient temperature fields in the domain up to  $t = 14$  for  $Ra = 6 \times 10^8$ ,  $Pr = 7$  and  $A = 2$ ; (b) time evolution of the contours of transient streamfunction fields up to  $t = 14$  for  $Ra = 6 \times 10^8$ ,  $Pr = 7$  and  $A = 2$ .

equivalent accuracy [25]. With a non-staggered scheme all variables have the same discrete operators whereas a different operator must be used for each of the velocities and the scalar variables in a staggered mesh. Hence the use of the non-staggered approach leads to a considerable simplification in the programming. This scheme is described in detail by Armfield [25]. Finite volumes are used to convert differential terms in the governing equations to differences as follows. All second derivatives and linear derivatives are approximated by second-order central differences. The convective terms are approximated by a QUICK scheme [26]. The discretization produces the usual fringed block tridiagonal matrix operator, one for each

of the momentum, temperature and pressure equations. These are solved using an alternating direction implicit method.

### 2.3. Time integration

The time integration is accomplished using a second-order Crank–Nicholson predictor-corrector scheme in which the solution of the transport equations is carried out in the following way. First, all variables are known at  $t = n\Delta t$ . Second the temperature Eq. (4) is inverted to obtain an initial approximation to  $T^{n+1}$ , and using this value the two momentum Eqs. (2) and (3) are inverted, using an estimated pressure field, to obtain a

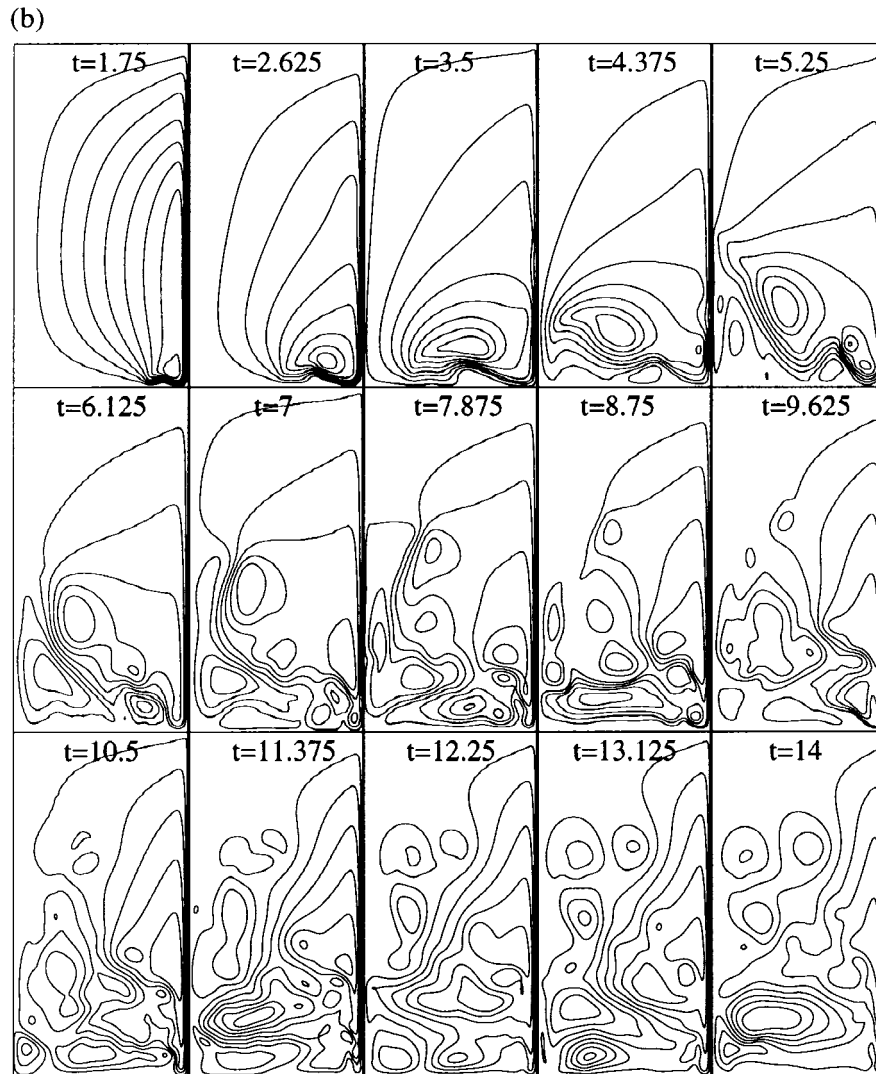


Fig. 3 (continued)

first approximation to  $u^{n+1}$  and  $v^{n+1}$ . A pressure correction equation derived from Eq. (1) is then solved to enforce continuity. Finally new estimates of  $u^{n+1}$  and  $v^{n+1}$  are obtained. This procedure is repeated until a preset divergence convergence criterion of  $1 \times 10^{-4}$  is met.

#### 2.4. Grid independence

To test the grid independence of the scheme the solution has been obtained on the basic mesh of  $99 \times 155$  defined above, which is the major mesh used in this study, and on two additional fine meshes, with the following parameters. The first fine mesh has one half the size at the wall and at the symmetry line, the same

grid expansion factor, and one half of the time step of the basic mesh of  $99 \times 155$ . This gives a grid of  $121 \times 181$  with approximately the same grid spacing in the core. The second mesh has one fifth the size at the wall and at the symmetry line, the same grid expansion factor, and one quarter of the time step of the basic mesh. This gives a grid of  $149 \times 217$ . Fig. 2a and b shows the temperature and vertical velocity profiles as a function of horizontal distance from the cold intrusion at midheight in the thermal boundary layer. The temperature and horizontal velocity profiles as a function of height in the lowest part of the domain at  $x = 0.4585$  are shown in Fig. 2c and d. All figures are for  $t = 0.875$ , after the thermal boundary layer is established and the cold intrusion has passed the

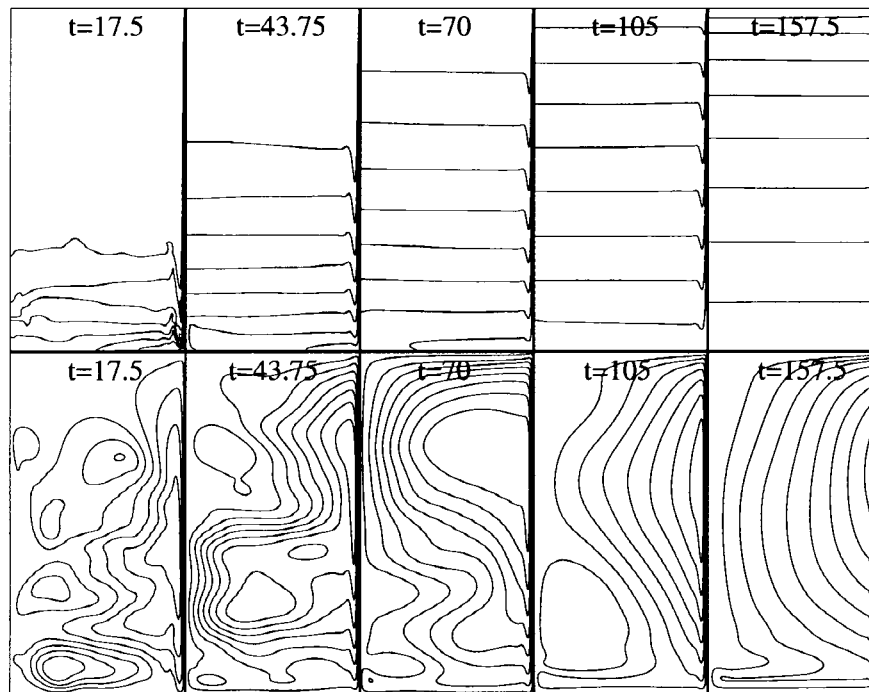


Fig. 4. Time evolution of the contours of transient temperature and streamfunction fields in the domain from  $t = 17.5$  to  $t = 157.5$  for  $Ra = 6 \times 10^8$ ,  $Pr = 7$  and  $A = 2$ .

$x = 0.4585$  point. In all cases, the variation between the three representations is very small, indicating that the basic mesh of  $99 \times 155$  is free of grid- and time-step-dependent errors.

### 3. Transient flow patterns

#### 3.1. Typical evolution of transient natural convection flows

To provide a comprehensive and direct perception of the transient evolving process of natural convection flow in the cylinder, we present in Figs. 3 and 4 the visualisation of the time evolution of transient flow parameters in the computational domain for  $Ra = 6 \times 10^8$ ,  $Pr = 7$  and  $A = 2$ . (In all contour figures, 10 equally-spaced contours between the maximum and minimum values are shown, therefore, for temperature, contours between 0 and  $-1$  are shown). From these figures, it is seen that when the sidewall is cooled impulsively to  $T = -1$ , a vertical thermal boundary layer develops very rapidly on the sidewall. After the full development of the vertical thermal boundary layer, a cold intrusion begins to form and moves continuously along the bottom wall towards the symmetry line. This phenomena is also observed by others [8]. As the intrusion approaches the symmetry line, its nose

increases in size and the shape changes gradually due to the interaction between the intrusion and the surrounding ambient fluid in the domain. Meanwhile, waves are travelling down the vertical thermal boundary layer, forming crests in the temperature fields as shown in Fig. 3a, which are believed to be initiated as a thermal boundary layer instability travelling down the vertical layer following the start-up of the thermal boundary layer [8,27–29]. When the intrusion nose approaches the symmetry line, its size grows sharply, and extends substantially along the symmetry line, resulting in a vigorous interaction similar to a collision between the intrusion and the symmetry line. After that, the intrusion falls down along the symmetry line after it has lost its upward momentum to the ambient fluid. The colliding intrusion reverses and moves back towards the sidewall. Consequently, this portion of the intrusion interacts with the newly-formed colder intrusion which is continuously being ejected from the cold sidewall and moving underneath the reversing fluid towards the symmetry line, forming a complicated interaction between the intrusions in the lower part of the domain. Prior to the arrival of the reversed intrusion, waves travelling down the vertical thermal boundary layer enter the intrusion and dissipate, further complicating the flow patterns. When the reversed intrusion approaches the sidewall, it interacts with the lower part of the vertical boundary layer,

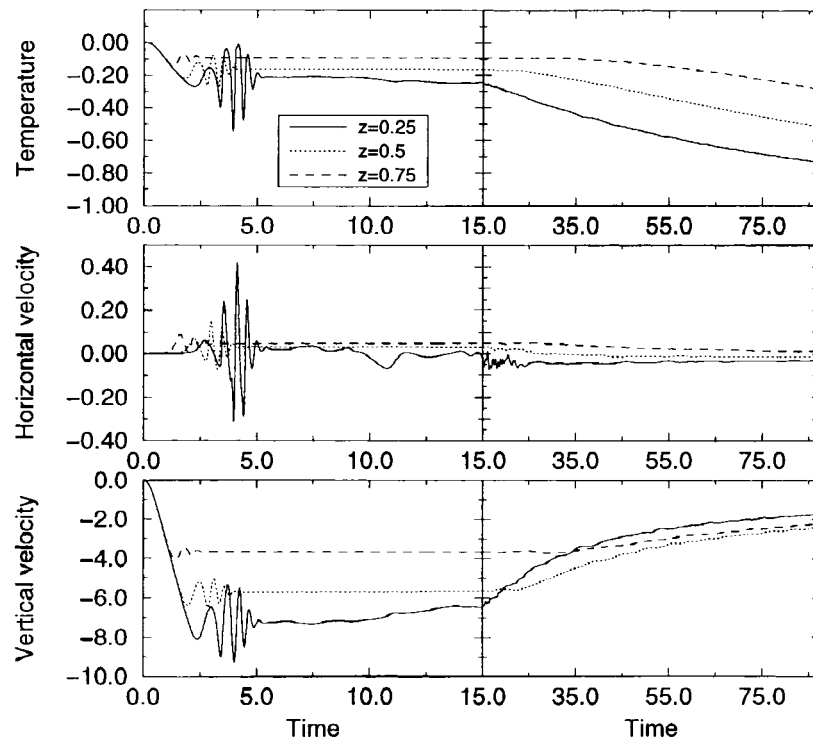


Fig. 5. Time traces of temperature, horizontal and vertical velocities at points  $r = 0.493$ ,  $z = 0.25$ ;  $r = 0.493$ ,  $z = 0.5$ ; and  $r = 0.493$ ,  $z = 0.75$  in the vertical region.

resulting in a perturbation travelling up the thermal boundary layer. Due to the balancing of buoyancy and momentum, heat and mass transfer occurs continuously among the cold intrusion, the surrounding ambient fluid and other intrusions. The cold intrusion loses its momentum but increases its temperature gradually in its back and forth passage between the sidewall and the symmetry line in the lower part of the domain. This same procedure is experienced by the successively produced new intrusions and this process acts to generate the temperature stratification in the interior. Gradually, the unsteady natural convection flow and the generation of the stratification in the domain will transit to a quasi-steady state.

In Fig. 4, it is clearly demonstrated that the flow is approaching a quasi-steady stratification, but at a gradually reduced rate due to the successively decreased driving buoyancy. The vertical thermal boundary layer gradually becomes thicker and its downward moving speed reduces progressively as the local  $Ra$  becomes smaller due to the decrease of the temperature difference between that on the sidewall and that inside the cylinder.

It is evident from these results that it is helpful to divide the evolution of natural convection flow in the domain into two specific stages, namely the unsteady

stage and the quasi-steady stage, respectively, as the transient flows have considerably different patterns at these stages. It is also found that vigorous flow activities take place mainly in the vertical boundary layer on the sidewall and in the lower part of the domain where the intrusions are embedded. For brevity, the first region is named as the vertical region and the other as the horizontal region.

### 3.2. Transient flow features: the unsteady stage

The initial flow at this stage is characterized by the development of the vertical thermal boundary layer on the sidewall. To get more detailed information about the development of the vertical thermal boundary layer, we present in Fig. 5 the time traces of temperature and velocities at three specific points which are in the vertical region. It is observed that the full development of the vertical thermal boundary layer on the sidewall takes a time of about 2 for the case considered here. It is evident that conduction dominates during this initial flow regime. After that, waves travel down the boundary layer, clearly seen in Fig. 3a as the crests in the temperature contours at  $t = 3.5$ , 4.375 and 5.25, and in Fig. 5 where wavelike traces of temperature and velocities are recorded. These waves may also be seen

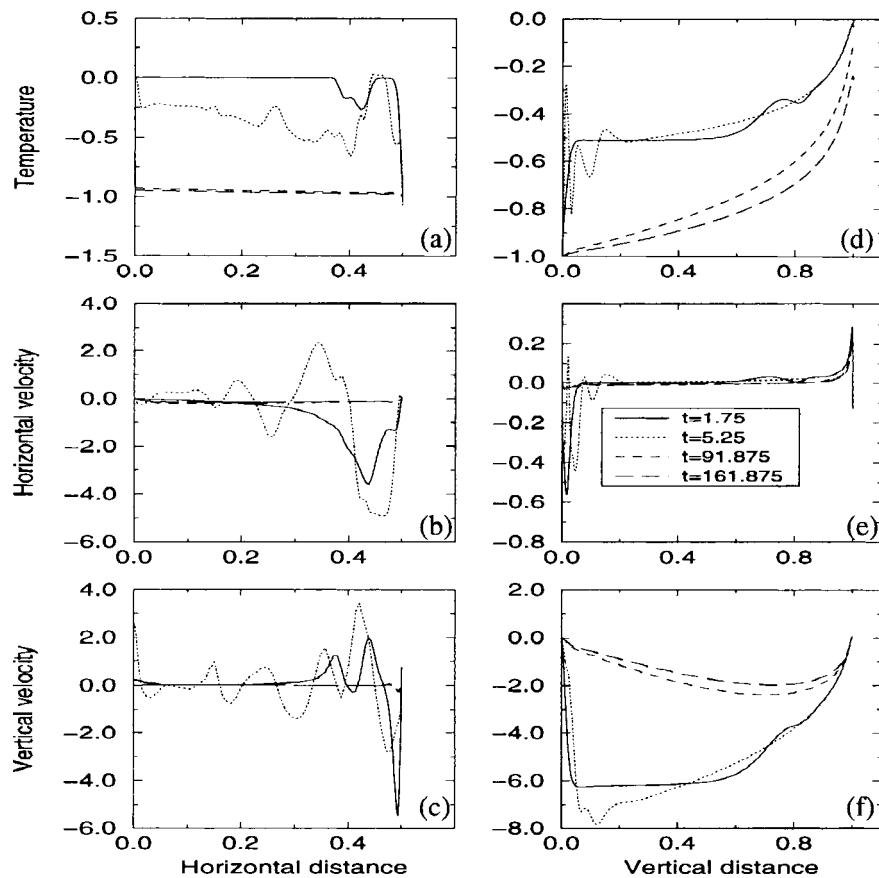


Fig. 6. Profiles of transient temperature, horizontal and vertical velocities along horizontal distances at  $z = 0.02$  in the horizontal region (a–c) and along vertical distances at  $r = 0.496$  in the vertical region (d–f) at  $t = 1.75, 5.25, 91.875$  and  $161.875$  respectively.

in Fig. 6 at time  $t = 5.25$ , which shows the profiles of temperature and velocities along horizontal distances in the horizontal region and along vertical distances in the vertical region at different times. Each peak in the signal shown in the figures corresponds to the passage of a single wave crest past the position at which the trace is recorded. Thus the two crests visible in Fig. 3a when  $t = 3.5$  and  $4.375$  correspond to the first two peaks in Fig. 5. It is also evident that the amplitude of the wave increases with the passage down the vertical thermal boundary layer, and that as a result the number of discernible crests increases. These waves are similar to those observed at start-up in a rectangular cavity with differentially heated sidewalls [6]. In that case, the flow also exhibits a second set of waves resulting from the striking of the hot intrusion coming from the heated sidewall on the top of the thermal boundary layer on this cooled sidewall. This second set of waves have a much bigger amplitude and are the major travelling waves in the boundary layer for the rectangular cavity case. In our case, however, as no hot intrusion strikes the top of the thermal boundary

layer on the cooled sidewall no second set of waves travel down the boundary layer. But as the reversed cold intrusion strikes the lower part of the boundary layer, a perturbation is generated which then travels up the thermal boundary layer. After the travelling and dissipation of waves and perturbations, the traces of temperature and velocities become smooth gradually, as clearly shown in Figs. 5 and 6, indicating that flows in the vertical thermal boundary layer are approaching the quasi-steady stage.

In the horizontal region, the temperature contours in Fig. 3a show that the nose of the first cold intrusion at  $t = 1.75$  is located at about  $r = 0.365$  so that a perturbation to the profiles is recorded in Fig. 6. This perturbation is also shown in Fig. 7, where the time traces of temperature and velocities at three specific points in the horizontal region are recorded, at  $r = 0.375$  where the recording point is just inside the intrusion crest, but no perturbation is found at the other locations  $r = 0.125$  and  $0.25$  as the nose of the cold intrusion has not yet passed there. At  $t = 5.25$ , the nose of the intrusion reaches the symmetry line and the collision

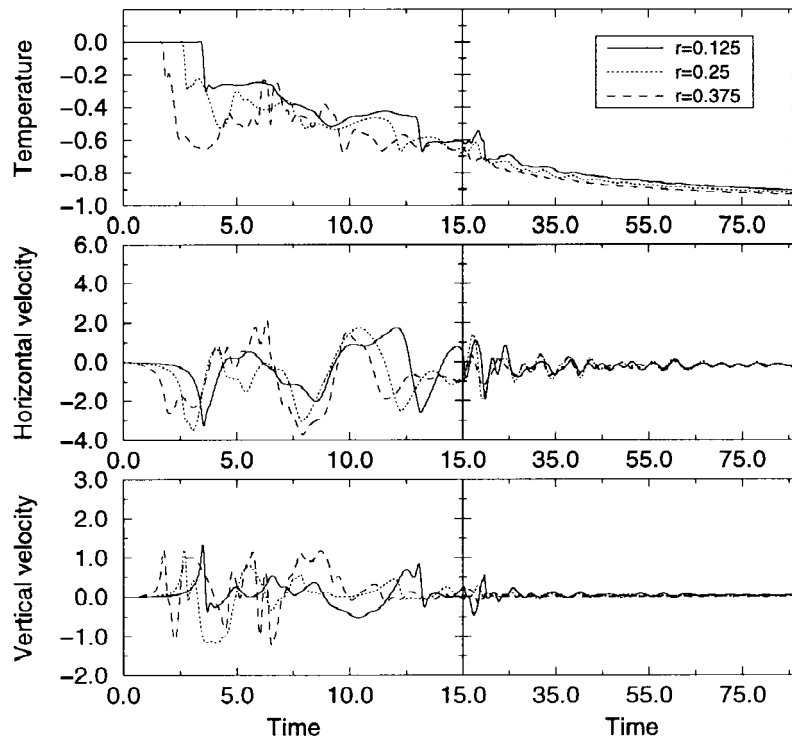


Fig. 7. Time traces of temperature, horizontal and vertical velocities at points  $r = 0.125$ ,  $z = 0.02$ ;  $r = 0.25$ ,  $z = 0.02$ ; and  $r = 0.375$ ,  $z = 0.02$  in the horizontal region.

occurs, resulting in sharp changes to the horizontal velocity in both amplitude and direction and a sharp increase in the vertical velocity amplitude, as evidently seen in Fig. 7. Meanwhile, it is found from Fig. 3a that the first travelling wave in the vertical region has just passed the right corner of the domain and finally dissipated in the cold intrusion, resulting in a big perturbation to temperature and velocities in the horizontal region. After the passage of the first wave into the horizontal region and before the coming of the second wave, an eddy is seen to form at the lower right corner of the domain which results in the sharp changes in temperature and velocities there. When the second travelling wave in the vertical region is approaching the right corner, a small perturbation in the horizontal region is generated. But at the same time, the intrusion nose is reversed by the symmetry line and then moves towards the cold sidewall. On its way back to the sidewall, it interacts with the surrounding ambient fluid and the intrusions underneath, strikes the lower part of the vertical boundary layer, and then moves back towards the symmetry line. This procedure is repeated continually in the horizontal region which, together with the travelling and dissipation of waves in the horizontal region, result in the consequent wavelike traces

and profiles of temperature and velocities as shown in Figs. 6 and 7.

### 3.3. Transient flow features: the quasi-steady stage

From Fig. 5, it is seen that after the passage of the waves the traces of temperature and velocities in the vertical region are smooth, indicating that the flow inside the vertical region is approaching a quasi-steady state. In the horizontal region, the flow takes a much longer time to approach a quasi-steady state. As the flow inside the horizontal region approaches the quasi-steady state, the temperatures at the three points gradually approach their final value, that is,  $T = -1$ , and the horizontal and vertical velocities approach 0, indicating a gradually reduced driven force of buoyancy due to the decreasing  $\Delta T$  and local  $Ra$  on the wall. The nearly horizontal profiles shown in Fig. 4 from  $t = 43.75$  on and those shown in Fig. 6 at  $t = 91.875$  and  $161.875$  show the development of a stratification inside the cylinder when the flow is approaching its quasi-steady state. Subsequently, the cylinder is continually filled with stratified fluid. At a specific time, the fluid inside the cylinder will be fully stratified. During the whole process of stratification

and after that, there is no vigorous flow activity except in the vertical region where the quasi-steady boundary-layer flows are maintained at a gradually reduced scale, and in the horizontal region where a very slow movement of the fluid is observed. After the interior fluid is fully stratified the flow continues to develop very slowly until all the interior fluid is at the temperature of the cooled wall and the system is again quiet.

#### 4. Scaling

The temporal and spatial scales for the development of the vertical thermal boundary layer on the sidewall and the stratification in the cylinder are important parameters that illustrate the transient flow features.

##### 4.1. Development of thermal boundary layer

After Patterson and Imberger [4], the time scale for the development of the vertical thermal boundary layer is  $t^* \sim H^2/(\kappa Ra^{1/2})$ , with boundary layer thickness  $\delta_T^* \sim H/Ra^{1/4}$  and velocity  $v^* \sim (\kappa Ra^{1/2})/H$ . Similarly, the time, velocity and thickness scales for the thermal boundary layer for full development at each height  $z^*$  are as follows:

$$t_z^* \sim \frac{(H - z^*)^2}{\kappa Ra_{z^*}^{1/2}} = \frac{H^2}{\kappa Ra^{1/2}} \left(1 - \frac{z^*}{H}\right)^2, \tag{9}$$

$$v_z^* \sim \frac{\kappa Ra_{z^*}^{1/2}}{(H - z^*)} = \frac{\kappa Ra^{1/2}}{H} \left(1 - \frac{z^*}{H}\right)^{-1/2}, \tag{10}$$

$$\delta_{Tz}^* \sim \frac{(H - z^*)}{Ra_{z^*}^{1/4}} = \frac{H}{Ra^{1/4}} \left(1 - \frac{z^*}{H}\right)^{1/4}. \tag{11}$$

where the local Rayleigh number is defined as

$$Ra_{z^*} = \frac{g\beta\Delta T(H - z^*)^3}{\nu\kappa} = Ra \frac{(H - z^*)^3}{H^3}. \tag{12}$$

Hence, the dimensionless time, velocity and thickness scales of the thermal boundary layer for full development at each height  $z$  are as follows:

$$t_z \sim (1 - z)^{1/2}, \tag{13}$$

$$v_z \sim (1 - z)^{1/2}, \tag{14}$$

$$\delta_{Tz} \sim \frac{(1 - z)^{1/4}}{Ra^{1/4}}. \tag{15}$$

The boundary layer is fully developed over the entire

wall when  $z = 0$ , giving a non-dimensional time scale for full development of  $t \sim 1$ , velocity scale  $v \sim 1$  and thickness  $\delta_T \sim Ra^{-1/4}$ .

##### 4.2. Time scale for full stratification

After the development of the vertical thermal boundary layer, the cylinder is gradually filled with stratified fluid, as observed in the last section. The rate of filling depends on the rate of fluid flow through the thermal boundary layer at the current filled height  $z$  as shown in Fig. 8, which shows a schematic for the filling with stratified fluid in the cylinder. The flux  $Q$  through the boundary layer at  $z$  is

$$Q \sim \frac{2\pi}{A} \delta_T(z) v(z) = \frac{2\pi}{A} \frac{(1 - z)^{3/4}}{Ra^{1/4}}, \tag{16}$$

where  $1/A$  is the cylinder radius and it is assumed that  $\delta_T \ll 1/A$ . The rate of change of the filled height  $z$  is then

$$(2A)^{-1} \frac{dz}{dt} \sim \frac{(1 - z)^{3/4}}{Ra^{1/4}}, \quad \text{with } z(0) = 0. \tag{17}$$

Solving this ordinary differential equation for  $z$  gives

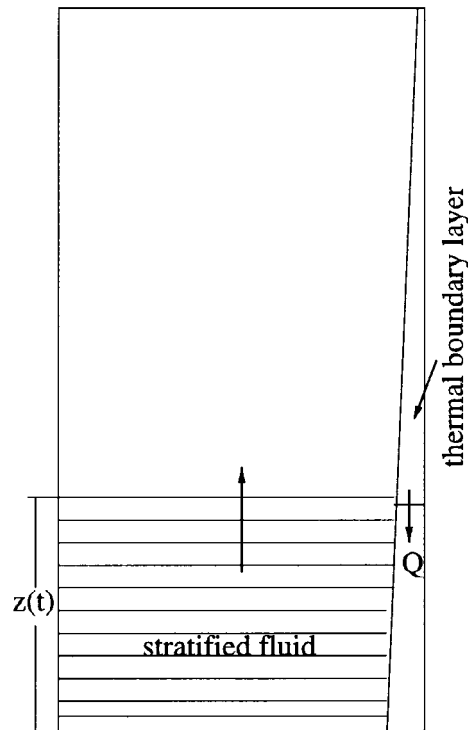


Fig. 8. Schematic of filling with stratified fluid in the cylinder.

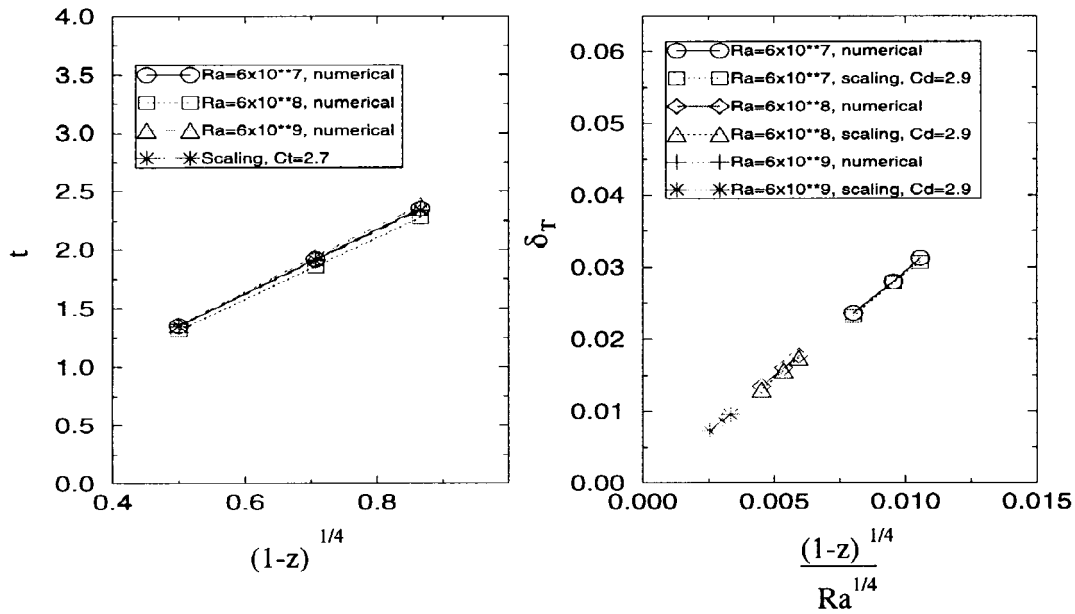


Fig. 9. Plots of numerically simulated and scaled time and thickness of vertical thermal boundary layer against the height for  $Ra = 6 \times 10^7, 6 \times 10^8$  and  $6 \times 10^9$ .

$$z(t) = 1 - \left(1 - \frac{C_s At}{Ra^{1/4}}\right)^4, \tag{18}$$

where  $C_s$  is a constant of proportionality.

The cylinder will be fully stratified when  $z(t)=1$ , giving the time scale

$$t_s = \frac{Ra^{1/4}}{C_s A}. \tag{19}$$

4.3. Comparison between numerical and scaling results

For the cases considered above, the vertical thermal boundary layer on the sidewall reached full development over its entire height at the time of about 2, as shown in Fig. 5. This observation is in good agreement with the scaling result  $t \sim 1$ . To validate the scaling results in a more general range, we conducted further numerical simulations. In Fig. 9, the numerically simulated and scaled time and thickness of the vertical thermal boundary layer against the height  $z$  are depicted for  $Ra = 6 \times 10^7, 6 \times 10^8$  and  $6 \times 10^9$ . The time shown is the time at which the boundary reached full development at that height, and  $\delta_T$  is the boundary layer thickness at full development at that height. It is seen that the time development is well predicted by the scaling with the constant of proportionality being  $C_t=2.7$ . The boundary layer thickness  $\delta_T$  as a function of  $z$  is also well predicted by the scaling at each  $Ra$  with the constant of proportionality  $C_d=2.9$ . In Figs. 10 and 11, the numerically simulated and scaled filling

height against the filling time and numerically simulated and scaled time for full stratification against  $Ra$  are shown respectively for six combinations of  $Ra$  and  $A$ . The variation of filling height with time, shown in Fig. 10, is very well predicted by the scaling with the

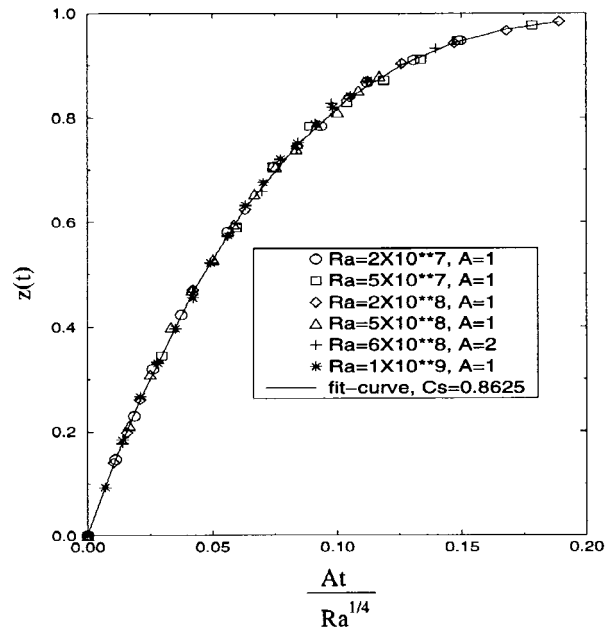


Fig. 10. Plot of numerically simulated and scaled filling height against the filling time for six Rayleigh numbers.

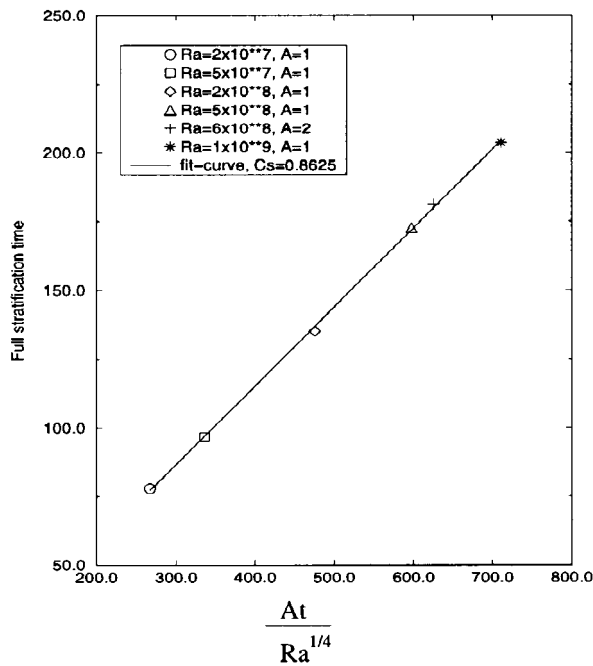


Fig. 11. Plot of numerically simulated and scaled time for full stratification against  $Ra$  for six Rayleigh numbers.

constant of proportionality  $C_s=0.8625$ . Similarly the time to full stratification, shown in Fig. 11, is very well predicted by (19) with the same constant.

## 5. Conclusions

Numerical solutions are obtained for the transient process of cooling-down and stratifying the fluid inside a vertical circular cylinder when its sidewall is set impulsively to a cold temperature. Visualisation of the transient evolving processes for  $Ra = 6 \times 10^8$  at both the unsteady stage and the quasi-steady stage provides a comprehensive and direct perception of the transient evolving flow patterns. The numerical simulations reveal that the flow has considerably different transient features at these two specific stages and vigorous flow activities mainly occur in the vertical thermal boundary layer on the sidewall and the horizontal region, the region in the lower part of the domain where the cold intrusion flows are embedded. The flows calculated here have higher Rayleigh numbers than those considered by previous workers, however the basic flow development remains the same. The primary difference is the considerable increase in activity in the intrusion region. The scalings for the total development time for the boundary layer and for the stratification obtained here are identical to those obtained previously in [23], where the boundary layer was labelled phase I and the

stratification was labelled phase III. Phase II was associated with a density inversion that does not occur in the flow considered here. In the present investigation scalings have also been obtained for the rate of development of the boundary layer and the stratification, and these have been shown to agree very well with the numerical simulations. Proportionality constants for each of the scalings have been obtained and shown to provide accurate prediction of the flow over a large range of Rayleigh numbers.

## Acknowledgements

We thank Professor J. C. Patterson for his helpful discussion. The financial support of an AusAID Scholarship for W. L. is gratefully acknowledged.

## References

- [1] G.K. Batchelor, Heat transfer by free convection across a closed cavity between vertical boundaries at different temperature, *Q. J. Appl. Maths* 12 (1954) 209–233.
- [2] I. Catton, Natural convection in enclosures, in: *Proceedings of the Sixth International Heat Transfer Conference*, vol. 6, Hemisphere, Washington, DC, 1978, p. 13–43.
- [3] S. Ostrach, Natural convection heat transfer in cavities and cells, in: *Proceedings of the Seventh International Heat Transfer Conference*, vol. 1, Hemisphere, Washington, DC, 1982, p. 365–379.
- [4] J.C. Patterson, J. Imberger, Unsteady natural convection in a rectangular cavity, *Journal of Fluid Mechanics* 100 (1980) 65–86.
- [5] V.F. Nicolette, K.T. Yang, Transient cooling by natural convection in a two-dimensional square enclosure, *International Journal of Heat and Mass Transfer* 28 (1985) 1721–1732.
- [6] S.G. Schladow, J.C. Patterson, R.L. Street, Transient flow in a side-heated cavity at high Rayleigh number: a numerical study, *Journal of Fluid Mechanics* 200 (1989) 121–148.
- [7] J.M. Hyun, Effect of the Prandtl number on heatup of a stratified fluid in an enclosure, *ASME Journal of Heat Transfer* 107 (1985) 982–984.
- [8] J.C. Patterson, S.W. Armfield, Transient features of natural convection in a cavity, *Journal of Fluid Mechanics* 219 (1990) 469–497.
- [9] S.W. Armfield, J.C. Patterson, Direct simulation of wave interactions in unsteady natural convection in a cavity, *International Journal of Heat and Mass Transfer* 34 (1991) 929–940.
- [10] S.W. Armfield, J.C. Patterson, Wave properties of natural-convection boundary layers, *Journal of Fluid Mechanics* 239 (1992) 195–211.
- [11] S.W. Armfield, R. Janssen, A direct boundary-layer stability analysis of steady-state cavity convection flow,

- International Journal of Heat and Fluid Flow 17 (1996) 539–546.
- [12] R. Janssen, S.W. Armfield, Stability properties of the vertical boundary layers in differentially heated cavities, *International Journal of Heat and Fluid Flow* 17 (1996) 547–556.
- [13] J.M. Hyun, Unsteady buoyant convection in an enclosure, *Advances in Heat Transfer* 24 (1994) 277–320.
- [14] S. Xin, P. Le Quéré, Direct numerical simulations of two-dimensional chaotic natural convection in a differentially heated cavity of aspect ratio 4, *Journal of Fluid Mechanics* 304 (1995) 87–118.
- [15] A.M.H. Brooker, J.C. Patterson, S.W. Armfield, Non-parallel linear stability analysis of the vertical boundary layer in a differentially heated cavity, *Journal of Fluid Mechanics* 352 (1997) 265–281.
- [16] D.R. Otis, J. Roessler, Development of stratification in a cylindrical enclosure, *International Journal of Heat and Mass Transfer* 30 (1987) 1633–1636.
- [17] T. Sakurai, T. Matsuda, A temperature adjustment process in a Boussinesq fluid via a buoyancy-induced meridional circulation, *Journal of Fluid Mechanics* 54 (1972) 417–421.
- [18] M.C. Jischke, R.T. Doty, Linearized buoyant motion in a closed container, *Journal of Fluid Mechanics* 71 (1975) 729–754.
- [19] J.M. Hyun, W.W. Fowles, A. Warn-Varnas, Numerical solutions for the spin-up of a stratified fluid, *Journal of Fluid Mechanics* 117 (1982) 71–90.
- [20] J.M. Hyun, Transient buoyant convection of a contained fluid driven by the changes in the boundary temperatures, *ASME Journal of Applied Mechanics* 52 (1985) 193–198.
- [21] J.M. Hyun, H.K. Choi, Transient cool down of a gas in a closed container, *J. Thermophys. Heat Transfer* 3 (1989) 441–446.
- [22] J.M. Hyun, Transient process of thermally stratifying an initially homogeneous fluid in an enclosure, *International Journal of Heat and Mass Transfer* 27 (1984) 1936–1938.
- [23] H.S. Kwak, K. Kuwahara, J.M. Hyun, Convective cool-down of a contained fluid through its maximum density temperature, *International Journal of Heat and Mass Transfer* 41 (1998) 323–333.
- [24] S.V. Patankar, in: *Numerical Heat Transfer and Fluid Flow*, Hemisphere, Washington, DC, 1980, p. 126.
- [25] S.W. Armfield, Finite difference solutions of the Navier–Stokes equations on staggered and non-staggered grids, *Computers Fluids* 20 (1991) 1–17.
- [26] B.P. Leonard, A stable and accurate convective modeling procedure based on quadratic upstream interpolation, *Comp. Meth. Appl. Mech. Engng.* 19 (1979) 59–98.
- [27] S. Paolucci, D.R. Chenoweth, Transition to chaos in a differentially heated vertical cavity, *Journal of Fluid Mechanics* 201 (1989) 379–410.
- [28] P. Le Quere, Transition to unsteady natural convection in a tall water-filled cavity, *Phys. Fluids A* 2 (1990) 503–515.
- [29] A.E. Gill, A. Davey, Instabilities of a buoyancy driven system, *Journal of Fluid Mechanics* 35 (1969) 775–798.